Letter

Emission of fast-propagating spin waves by an antiferromagnetic domain wall driven by spin current

Roman V. Ovcharov,[1] B. A. Ivanov,[2,3] Johan Åkerman,[1,4,5] and Roman S. Khymyn[1]
[1]*Department of Physics, University of Gothenburg, Gothenburg 41296, Sweden*
[2]*Institute of Magnetism of NASU and MESU, Kyiv 03142, Ukraine*
[3]*William H. Miller III Department of Physics and Astronomy, Johns Hopkins University, Baltimore, Maryland 21218, USA*
[4]*Center for Science and Innovation in Spintronics, Tohoku University, Sendai 980-8577, Japan*
[5]*Research Institute of Electrical Communication, Tohoku University, Sendai 980-8577, Japan*

(Received 25 March 2024; revised 2 April 2024; accepted 3 April 2024; published 16 April 2024)

Antiferromagnets (AFMs) have great benefits for spintronic applications such as high frequencies (up to THz), high speeds (up to tens of km/s) of magnetic excitations, and field-free operation. Advanced devices will require high-speed propagating spin waves (SWs) as signal carriers, i.e., SWs with high k vectors, the excitation of which remains challenging. We show that a domain wall (DW) in anisotropic AFM driven by the spin current can be a source of such propagating SWs with high frequencies and group velocities. In the proposed generator, the spin current, with polarization directed along the easy anisotropy axis, excites the precession of the Néel vector within the DW. The threshold current is defined by the value of the anisotropy in the hard plane, and the frequency of the DW precession is tunable by the strength of the spin current. We show that the above precession of spins inside the DW leads to robust emission of high-frequency propagating SWs into the AFM strip with very short wavelengths comparable to the exchange length, which is hard to achieve by any other method.

DOI: 10.1103/PhysRevB.109.L140406

Introduction. Spin-transfer-torque and spin-Hall auto-oscillators (AOs) based on ferromagnetic materials (FMs) are well-established devices in modern spintronics and have a great potential for advanced signal and data processing [1–4]. For example, owing to their highly nonlinear behavior, they are promising in neuromorphic computing applications, such as image or sound recognition [5–7]. Such complex tasks require large arrays of strongly mutually coupled AOs that can be achieved by direct exchange, magnetodipolar interactions, or spin waves (SWs) propagating between individual AOs [8–13]. The latter has special advantages since SWs can carry signals on large distances and be additionally processed in the inter-AO space [7,14,15]. Despite the above benefits, the FM AOs have significant drawbacks, such as the necessity of externally applied strong magnetic field, low operational frequencies, which are usually limited by a few tens of GHz [16], and low velocity of the emitted SWs, which are of the order of 1 km/s.

Recently, it was proposed to use antiferromagnetic materials (AFM) instead of FM to eliminate the above issues [17–25]. AFM AOs can operate in the THz frequency range and do not require an external magnetic field due to the well-known feature of the AFM spin dynamics, the utilization of the internal exchange field or so-called exchange amplification [26–28]. The velocities of the SWs in AFMs can reach dozens of km/s [29], which is promising for the fast signal/data transduction between AOs. However, substantially short wavelengths of the excited magnons are required to achieve such high velocities. The dispersion relation for the propagating SWs in AFM reads as $\Omega = \sqrt{\omega_0^2 + c^2k^2}$ [where ω_0 is the frequency of AFM resonance (AFMR), c is the maximum group velocity of magnons, and k denotes a wave vector]. Thus, the group SW velocity, $v_{gr} = \partial\Omega/\partial k$, tends to zero for a small k, and one is interested in the case $k \gtrsim \omega_0/c$, which corresponds to the wavelength of a few tens of nanometers for the typical AFMs, such as orthoferrites [30] (40 nm for $\omega_0/2\pi = 500$ GHz, $c = 20$ km/s). The excitation of such short coherent waves is a fundamental problem of modern magnonics since it requires an ultracompact source of magnons [31], despite different finesses, such as the usage of higher-order radial and azimuthal modes.

Here, we propose to employ a spin-current-driven domain wall (DW) in an AFM as an ultracompact source of the propagating coherent SWs. We demonstrate theoretically and by micromagnetic simulations that the simple spin texture, such as an AFM DW, driven by spin current [32,33], can be a source of the propagating SWs with substantially high frequencies and short wavelengths, comparable to the exchange length of the AFM. We consider a device, schematically shown in Fig. 1, which is based on a thin film of an AFM with easy-axis anisotropy and n-fold rotational symmetry in the hard plane. In the proposed generator, the spin current flowing from the adjunct layer with the polarization along the principal axis excites the precession of the Néel vector within the DW. We assume the finite size of the spin-current source with a width L located directly under a DW. The setup for the spin-current source can vary depending on the dielectric

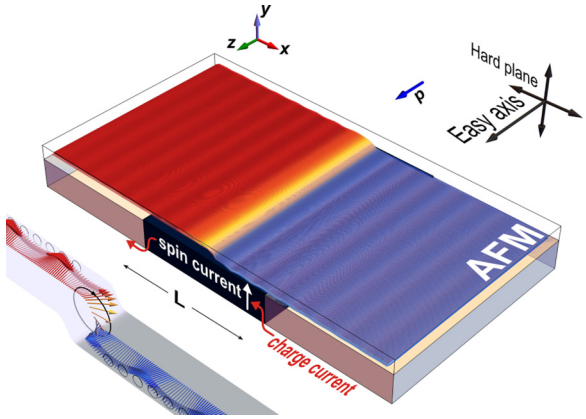

FIG. 1. Schematic representation of the proposed ultrashort SW generator. The spin-torque source (shown by a dark blue bar with width L) is positioned at the device's center beneath the AFM DW. Charge current flow through a heavy metal leads to spin-current injection at the interface (due to the spin-Hall effect) with polarization $\mathbf{p}$ aligned with the easy axis. The spin-current application induces precession of the Néel vector within the DW in the hard plane with n-fold symmetry. This precession results in the emission of SWs, as schematically shown in the lower-left-hand corner.

properties of an AFM. For insulating AFMs, a heavy metal layer can be employed, where a flow of a charge current generates a spin current at the interface via the spin-Hall effect, as illustrated in Fig. 1. For metallic AFMs, an adjacent layer of a ferromagnet can serve as a spin polarizer. In this arrangement, charge and spin currents flow perpendicular to the film, with the polarization of the spin current determined by the direction of magnetization in the ferromagnetic layer. The threshold current of the excitation is defined by the value of the anisotropy in the hard plane, and the frequency of the DW precession ω is tunable by the strength of the spin current. We show that the above precession of the DW leads to the excitation of two modes of magnons with the frequencies $\Omega = (n \pm 1)\omega$, where n is the order of the anisotropy. A robust emission of the propagating SWs into the AFM strip occurs when $(n \pm 1)\omega > \omega_0$, where ω_0 defines the frequency of AFM resonance. Consequently, the maximum achievable frequency of SWs is $(n+1)\omega_0$, which corresponds to very short wavelengths of the SW, comparable with the exchange length, especially for the hexagonal AFMs. The excitation of the high wave vectors is possible due to the substantially small width of the DW in AFM, which is hard to achieve by any other method.

Model. The low-energy dynamics of a collinear AFM can be described using the Lagrangian $\mathcal{L} = T - U$ for the Néel vector $\mathbf{l} = (\mathbf{M}_1 - \mathbf{M}_2)/M_s$, where $|\mathbf{M}_i| = M_s/2$ is the magnetization of the sublattice $i = 1, 2$ and M_s is the value of saturated AFM magnetization. The "kinetic" energy $T = (M_s/2\gamma\omega_{\rm ex})(\partial_t \mathbf{l})^2$ determines the inertial properties of the AFM spin dynamics, where $\omega_{\rm ex} = \gamma H_{\rm ex}$ is the frequency defined by the exchange field $H_{\rm ex}$ of the AFM, and γ is a gyromagnetic ratio. The "potential" term $U = (A/2)(\nabla \mathbf{l})^2 + w_a(\mathbf{l})$ is determined by nonuniform exchange (A) and anisotropy energy w_a. Expressing the Néel vector in spherical coordinates $\mathbf{l} = \{\sin\theta\cos\phi, \sin\theta\sin\phi, \cos\theta\}$, the anisotropy energy density reads

$$w_a = \frac{K}{2}\sin^2\theta + \frac{K_n}{n}\sin^n\theta\sin^2\left(\frac{n\phi}{2}\right), \tag{1}$$

where the first term defines uniaxial anisotropy of the easy-axis type ($K > 0$), and the second one defines an anisotropy in the hard plane ($K_n > 0$), for an AFM with an n-fold axis C_n. Here, the z axis is chosen along the easy axis of the AFM, $K > K_n$, and the ground state corresponds to $l_z \to \pm 1$ ($\theta = 0, \pi$).

A purely uniaxial AFM model ($K_n = 0$) possesses formal Lorentz invariance [28,34] with the characteristic velocity $c = \gamma\sqrt{H_{\rm ex}A/M_s}$ and degeneracy of the antiferromagnetic resonance (AFMR) frequency $\omega_0 = \gamma\sqrt{H_{\rm ex}K/M_s}$. The solution for a stationary DW with boundary conditions $l_z|_{\pm\infty} \to \pm 1$ can be found from the minimum of the potential energy U as $\cos\theta_0 = \tanh x/x_0$ and $\varphi = \varphi_s$, where $x_0 = \sqrt{A/K}$ is the thickness of stationary DW and angle ϕ_s determines the rotation of the $\mathbf{l}$ vector in the hard plane. The rotational dynamics of interest thus can be described by the transformation $\varphi = \omega t + \varphi_s$ and $x_0 \to \Delta(\omega) = x_0/\sqrt{1 - \omega^2/\omega_0^2}$, where ω denotes angular velocity of the Néel vector precession in a DW [28,34]. To induce the rotational dynamics, a spin current that is polarized along the easy axis of the AFM can be utilized. The frequency ω dependence on the current j is governed by the equilibrium between the total energy losses in the DW and the energy gained within the constrained region (with the width L, see Fig. 1) of the spin current's contact area [32],

$$\alpha\omega = \sigma j \tanh\left(\frac{L}{2x_0}\sqrt{1 - \frac{\omega^2}{\omega_0^2}}\right), \tag{2}$$

where α is an effective Gilbert damping, σ is a spin-torque efficiency, and j is a density of electric current. In the case of a large spin-torque source, $L \gg x_0$ and $\omega \ll \omega_0$, the frequency of the rotation is linearly proportional to the applied current $\omega = \sigma j/\alpha$.

Let us continue our analysis with the second term of Eq. (1)—namely, anisotropy in the hard plane K_n, that leads to the excitation of spin waves. In order to investigate the spin-wave excitation, we consider small perturbations of the initial DW solution as $\theta = \theta_0(x) + \vartheta(x,t)$ and $\varphi = \varphi_s + \omega t + \mu(x,t)/\sin\theta_0(x)$. It is convenient to combine polar and azimuthal perturbations into a single complex variable $\psi = \mu + i\vartheta$. Assuming a small value of the symmetry-reducing term $K_n \ll K$, one can obtain the linearized equation for ψ in the form [35] (see Supplemental Material [36] for the details)

$$\hat{H}_0\psi + \frac{1}{\omega_0^2 - \omega^2}\partial_t^2\psi - \frac{2i\omega\cos\theta_0}{\omega_0^2 - \omega^2}\partial_t\psi = B_n^+(\xi)e^{in\omega t} + B_n^-(\xi)e^{-in\omega t}, \tag{3}$$

where $\hat{H}_0$ is the Schrödinger operator with the reflectionless Pöschl-Teller potential $\hat{H}_0 = -\partial_\xi^2 + 1 - 2\cosh^2\xi$, $\xi = x/\Delta$. The left-hand side of Eq. (3) describes small-amplitude excitations in an AFM containing a precessing DW. The included type of potential created by a DW for linear SWs was already discussed for the FM as well as AFM materials. Particularly,

the emission of exchange SWs from a Bloch DW, excited by a microwave magnetic field, was predicted for FMs in Ref. [37]. For uniaxial AFMs, the above approach was employed in Ref. [38], where the propulsion of a DW by incoming SWs was demonstrated. The right-hand side of Eq. (3) represents a periodic driving "force" with frequencies $\pm n\omega t$ and corresponding amplitudes $B_n^{\pm}(\xi) = -iB_n \sin^{n-1}\theta_0(\cos\theta_0 \pm \sin\theta_0)/2$, where $B_n = K_n/2K(1-\omega^2/\omega_0^2)$ is proportional to the value of the anisotropy in the hard plane. Please note that superscripts indicate the sign of the corresponding frequency, i.e., the direction of ψ rotation.

The free solution of Eq. (3) can be represented in the form of a planar wave $\psi = e^{i(\tilde{k}\xi+\tilde{\Omega}t)}$, where $\tilde{k} = k\Delta$ is the rescaled wave vector and $\tilde{\Omega} = \Omega \pm \omega$ is the wave frequency in the rotating reference frame. At a large distance from the DW, $\tilde{k}$ and $\tilde{\Omega}$ are connected by the relation

$$\tilde{k}^2\big|_{\xi\to\pm\infty} = \frac{(\omega \mp \tilde{\Omega})^2 - \omega_0^2}{\omega_0^2 - \omega^2}, \tag{4}$$

which is a transformed version of the known dispersion law for spin waves $\Omega^2 = \omega_0^2 + c^2k^2$ in the observer's coordinate system.

As it follows from the right-hand side of the Eq. (3), $\psi(\xi,t)$ should be expressed as a linear combination of terms with both positive and negative frequencies $\pm n\omega t$. However, it is sufficient to consider one frequency sign since the part with the opposite sign is symmetric with respect to $\xi = 0$. Separating spatial and time variables as $\psi = \chi^{\pm}(\xi)e^{\pm in\omega t}$ the equation (3) can be written as

$$-\partial_\xi^2\chi^{\pm} + U_\omega^{\pm}(\xi)\chi^{\pm} = B_n^{\pm}(\xi), \tag{5}$$

for the spatial part $\chi^{\pm}(\xi)$, where $U_\omega^{\pm}(\xi)$ is a dimensionless potential for SWs created by a DW rotation and is given by

$$U_\omega^{\pm}(\xi) = 1 - \frac{2}{\cosh^2\xi} - \frac{n^2\omega^2}{\omega_0^2-\omega^2} \pm \frac{2n\omega^2}{\omega_0^2-\omega^2}\tanh\xi. \tag{6}$$

The function $B_n^{\pm}(\xi)$ in Eq. (5) defines the amplitude of a spin wave, while the potential $U_\omega^{\pm}(\xi)$ defines the condition for its propagation. Particularly, for the propagating SW in the form $\chi(\xi) \propto e^{\pm i\tilde{k}\xi}$ the wave vector acquires the real value $\tilde{k}^2 > 0$ when

$$U_\omega^{\pm}(\pm\infty) < 0. \tag{7}$$

Thus, Eq. (7) is a condition for a SW propagation with a wave vector $\tilde{k}^2$ given by the relation (4) with a substitution $\tilde{\Omega} \to n\omega$.

The potential $U_\omega^{\pm}$ depends on the frequency of DW rotation ω (see Fig. 2), which in turn can be controlled by the applied current in accordance with Eq. (2). Thus, by increasing the current, the condition for the emission is fulfilled when certain critical frequencies are exceeded:

$$\omega > \omega_{\rm cr}, \quad \omega_{\rm cr}^2 = \omega_0^2/(n\pm1)^2. \tag{8}$$

In general, critical frequencies (8) distinguish three frequency ranges of the DW precession. At low frequencies $\omega < \omega_0/(n+1)$ propagating SWs are not excited, since the wave vector k is purely imaginary. At $\omega_0/(n+1) < \omega < \omega_0/(n-1)$ only one branch of propagating SWs is emitted by a DW with a frequency $\Omega = (n+1)\omega$. At $\omega > \omega_0/(n-1)$ the second branch of SWs appears with frequency $\Omega = (n-1)\omega$. The third region is, however, absent for twofold anisotropy with $n = 2$, since corresponding frequencies lie below AFMR.

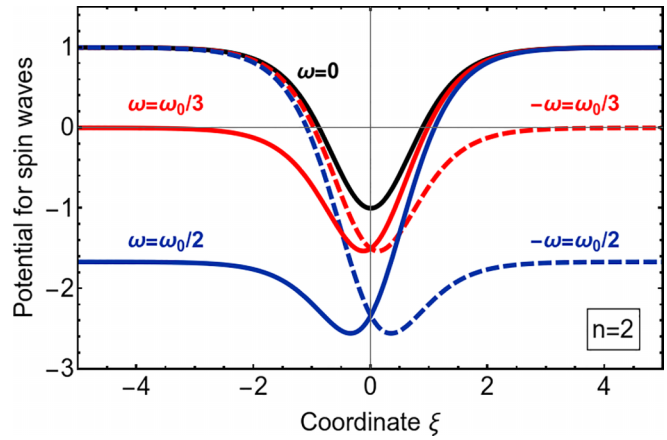

FIG. 2. Potential $U_\omega^{\pm}$ created by a precessing DW for SWs, given by Eq. (6), for a different frequency ω of a DW precession. Solid lines correspond to the positive sign of a SW frequency, while dashed lines correspond to the negative sign.

Micromagnetic simulations. To validate our analytical findings, we carried out micro-magnetic simulations using the MUMAX3 solver [39] for a system schematically shown in Fig. 1. The AFM film has lateral sizes 0.14×1.56 μm^2 with a thickness of 5 nm. The selected parameters used for the AFM correspond to the $DyFeO_3$ and are given as [30] $\alpha = 10^{-3}$, $M_s = 8.4 \times 10^5$ A/m, $A = 18.9$ pJ/m, $H_{\rm ex} = 670$ T, and the anisotropy constant along the easy axis $K = 300$ kJ/m^3. These parameters correspond to the characteristic speed $c = 22$ km/s, the frequency of the AFM resonance $\omega_0/2\pi = 0.45$ THz, and the width of a stationary DW $x_0 = 8$ nm. $DyFeO_3$ was chosen due to the relatively simple tunability of the second anisotropy K_2 in this material, for example, by temperature [40–42]. Particularly, at low temperatures, it is possible to achieve a uniaxial state [40] with $K_n = 0$, where two magnon modes are degenerated, and by varying temperature in the vicinity of this point, it is possible to tune K_2 in a wide range.

A spin-current source with a lateral size 0.14×0.1 μm^2 ($L = 100$ nm) is positioned under a DW at the center of the device, injecting a spin torque polarized along the easy axis of the AFM. The selected polarization of a spin torque does not induce translational DW movement. However, additional methods, such as nanoconstriction-based pinning, can be utilized to ensure DW placement beneath the current source [32]. The DW tends to be positioned in the center of the nanoconstriction, where it realizes the shortest length and, consequently, the lowest energy. This layout has the additional benefit of the highest current density at the center of the nanoconstriction, i.e., the maximum overlap of the applied spin current with a DW. Here, however, the rectangular geometry of the source is considered for a complete comparison with the analytical model. The frequency of the DW rotation is evaluated at the central location, where an initially relaxed DW is present. The frequencies of the excited SWs are measured at a distance of 300 nm from the DW.

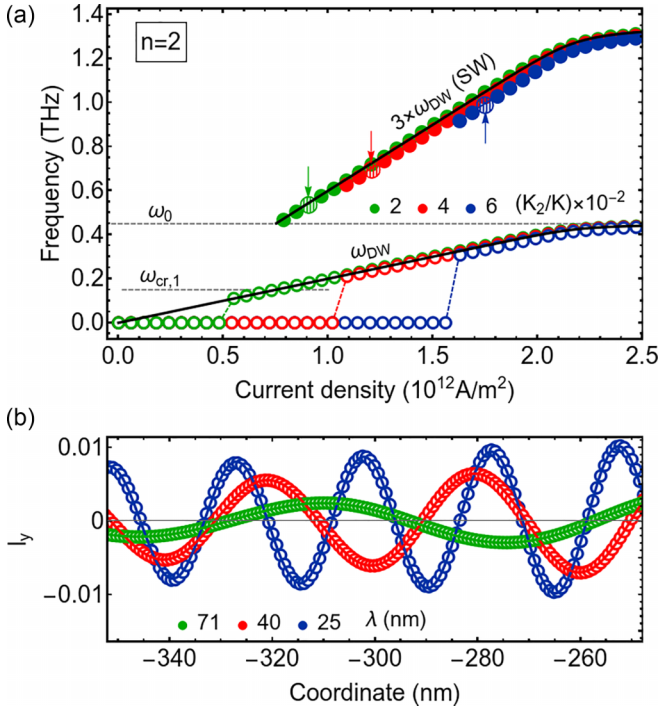

FIG. 3. The results of simulations for twofold anisotropy in a hard AFM plane, $n = 2$. (a) The frequency of the DW rotation (open circles) and emitted SWs (solid circles) are shown as a function of the applied current density for different values of K_2 anisotropy. Solid black lines are calculated analytically using Eq. (2). Angular frequency labels are employed for simplicity and correspond to the respective rotational frequencies $f = \omega/2\pi$. (b) The profiles of emitted SWs far from a DW with the extracted values of the wavelengths: $\lambda = 71$ nm (red), 40 nm (green), 25 nm (blue). The applied current density and frequencies of the displayed SWs are indicated by arrows of matching colors in (a).

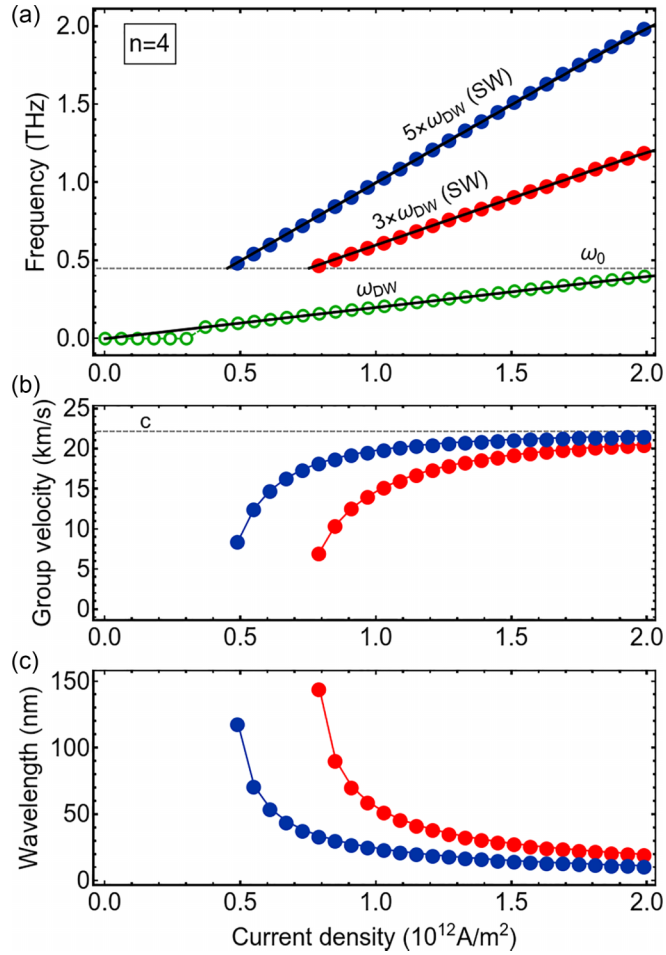

FIG. 4. The results of simulations for fourfold anisotropy in a hard AFM plane, $n = 4$. (a) The frequency of the DW rotation (open circles) and emitted SWs (solid circles) are shown as a function of the applied current density for $K_4/K = 2 \times 10^{-2}$. Solid black lines are calculated analytically using Eq. (2). (b) Group velocity and (c) wavelength of the excited SWs as a function of the applied current density.

Figure 3 shows the results of simulations with twofold anisotropy in the hard AFM plane, considering various values of K_2. The presence of K_2 anisotropy induces the excitation threshold current $\sigma j_{\text{th}} = \omega_2^2/(2\omega_{\text{ex}})$, where $\omega_n = \gamma\sqrt{H_{\text{ex}}K_n/M_s}$. In particular, for $K_2/K = 0.02$, the excitation starts at $j_{\text{th}} = 0.53 \times 10^{12}$ A/m^2 with frequency $\omega_{\text{th}} \simeq \sigma j_{\text{th}}/\alpha = \omega_n^2/(2\alpha\omega_{\text{ex}}) \approx 100$ GHz. With an increase in current, the frequency of DW rotation reaches the critical frequency $\omega_{\text{cr},1} = \omega_0/3 = 150$ GHz, leading to the detection of SWs at a large distance from the DW. The dependence of the DW frequency on the applied current is in good agreement with Eq. (2), despite being derived with the assumption $K_n/K \ll 1$. As predicted above, the frequency of the propagating SW is a multiple of the DW frequency with a factor of $n + 1 = 3$ and hence follows the scaled dependence (2) on the applied current.

Since increasing the anisotropy K_n leads to an increase in the threshold current j_{th}, the frequency of a DW precession at the threshold exceeds $\omega_{\text{cr},1}$ for high values of K_n. As a result, only SWs with a substantial frequency gap above AFMR can be excited in this case; see $K_n/K = 0.04$ and 0.06 in Fig. 3. Another outcome of raising K_n is the increase of the SW amplitude, since the driving term $B_n^{\pm} \propto K_n$ in Eq. (5). The SW radiation serves as an additional dissipation mechanism and results in a reduction of the measured DW frequency (and correspondingly the frequency of emitted SWs) as compared to the dependency (2). This effect is visible in Fig. 3 for $K_n/K = 0.06$.

The results for fourfold anisotropy with $K_4/K = 0.02$ are shown in Fig. 4. Here, all other parameters are left unchanged for the possibility of a direct comparison with the $n = 2$ case. The excitation threshold current for $n = 4$ is given by $\sigma j_{\text{th}} = \omega_4^2/(3\omega_{\text{ex}})$, which corresponds to $j_{\text{th}} = 0.35 \times 10^{12}$ A/m^2 and a frequency of $\omega_{\text{th}}/2\pi = 70$ GHz. Upon reaching the first critical frequency $\omega_{\text{cr},1} = \omega_0/5 = 90$ GHz, only SWs with a fivefold frequency are observed. As the current is further increased, the DW surpasses the subsequent critical frequency $\omega_{\text{cr},2} = \omega_0/3 = 150$ GHz, leading to the emission of SWs with a triple frequency as well.

Figures 4(b) and 4(c) show group velocity and a wavelength of emitted SWs as a function of applied current. Our simulation results suggest ultrahigh velocities, exceeding 10 km/s, even at low supercriticality, while at higher currents, the

velocity of emitted SWs is closely approaching the maximum value of 22 km/s. Such a result is extremely hard to achieve by any other method of excitation due to the extremely small wavelength $\simeq$10 nm [see Fig. 4(c)] of the magnon.

Discussion. One can note that Eq. (3) is derived for the conservative case, i.e., does not take dissipation and spin current into account. Thus, the emission of the SWs can be created by any mechanism, which leads to the corresponding spin precession in the DW, and spin torque induced by a current is one of them. Gilbert damping defines the frequency of the DW precession in accordance to Eq. (2) and also leads to the decay of the propagating SWs, as one can see in the inset of Fig. 3.

It is worth mentioning that the anisotropy in the hard plane is not the only mechanism that leads to the reduction of the DW dynamic symmetry [35]. The corresponding effect of the SW emission can occur in AFM with a specific form of the Dzyaloshinskii-Moriya interaction (DMI) characterized by a function $D(\theta, \phi)$. The forms of the functions $D(\theta, \phi)$ for many AFMs are detailed in Ref. [43]. The incorporation of DMI results leads to the term of a form $D(\theta) \sin n\omega t$ in the right-hand side of Eq. (3), which acts as a periodic driving "force," similarly to the effect of anisotropy.

To summarize, it has been shown theoretically and confirmed by micromagnetic simulations that the AFM DW, in which internal rotational dynamics is excited by a spin current, can be utilized as a generator of SWs with remarkably high frequencies and group velocities, which correspond to short wavelengths of the order of the AFM exchange length. The AFM DW, due to its small characteristic width, serves as an efficient generator of SWs that are difficult to excite by other methods. In addition, the application of such radiation for the synchronization of AFM oscillators with multiple DWs, where the dynamics is induced by the spin torque, is of particular interest.

Acknowledgments. This project is partly funded by the European Research Council (ERC) under the European Union's Horizon 2020 research and innovation programme (Grant TOPSPIN No. 835068) and the Swedish Research Council Grant No. 2016-05980.

[1] V. E. Demidov, S. Urazhdin, H. Ulrichs, V. Tiberkevich, A. Slavin, D. Baither, G. Schmitz, and S. O. Demokritov, Magnetic nano-oscillator driven by pure spin current, Nat. Mater. **11**, 1028 (2012).

[2] V. Demidov, S. Urazhdin, A. Zholud, A. Sadovnikov, and S. Demokritov, Nanoconstriction-based spin-Hall nano-oscillator, Appl. Phys. Lett. **105**, 172410 (2014).

[3] A. Slavin and V. Tiberkevich, Nonlinear auto-oscillator theory of microwave generation by spin-polarized current, IEEE Trans. Magn. **45**, 1875 (2009).

[4] T. Chen, R. K. Dumas, A. Eklund, P. K. Muduli, A. Houshang, A. A. Awad, P. Dürrenfeld, B. G. Malm, A. Rusu, and J. Åkerman, Spin-torque and spin-Hall nano-oscillators, Proc. IEEE **104**, 1919 (2016).

[5] J. Grollier, D. Querlioz, K. Camsari, K. Everschor-Sitte, S. Fukami, and M. D. Stiles, Neuromorphic spintronics, Nat. Electron. **3**, 360 (2020).

[6] M. Romera, P. Talatchian, S. Tsunegi, F. Abreu Araujo, V. Cros, P. Bortolotti, J. Trastoy, K. Yakushiji, A. Fukushima, H. Kubota *et al.*, Vowel recognition with four coupled spin-torque nano-oscillators, Nature (London) **563**, 230 (2018).

[7] M. Zahedinejad, A. A. Awad, S. Muralidhar, R. Khymyn, H. Fulara, H. Mazraati, M. Dvornik, and J. Åkerman, Two-dimensional mutually synchronized spin Hall nano-oscillator arrays for neuromorphic computing, Nat. Nanotechnol. **15**, 47 (2020).

[8] S. Kaka, M. R. Pufall, W. H. Rippard, T. J. Silva, S. E. Russek, and J. A. Katine, Mutual phase-locking of microwave spin torque nano-oscillators, Nature (London) **437**, 389 (2005).

[9] F. Mancoff, N. Rizzo, B. Engel, and S. Tehrani, Phase-locking in double-point-contact spin-transfer devices, Nature (London) **437**, 393 (2005).

[10] S. Sani, J. Persson, S. M. Mohseni, Y. Pogoryelov, P. Muduli, A. Eklund, G. Malm, M. Käll, A. Dmitriev, and J. Åkerman, Mutually synchronized bottom-up multi-nanocontact spin–torque oscillators, Nat. Commun. **4**, 2731 (2013).

[11] N. Locatelli, A. Hamadeh, F. Abreu Araujo, A. D. Belanovsky, P. N. Skirdkov, R. Lebrun, V. V. Naletov, K. A. Zvezdin, M. Muñoz, J. Grollier *et al.*, Efficient synchronization of dipolarly coupled vortex-based spin transfer nano-oscillators, Sci. Rep. **5**, 17039 (2015).

[12] A. Houshang, E. Iacocca, P. Dürrenfeld, S. R. Sani, J. Åkerman, and R. K. Dumas, Spin-wave-beam driven synchronization of nanocontact spin-torque oscillators, Nat. Nanotechnol. **11**, 280 (2016).

[13] R. Lebrun, S. Tsunegi, P. Bortolotti, H. Kubota, A. Jenkins, M. Romera, K. Yakushiji, A. Fukushima, J. Grollier, S. Yuasa *et al.*, Mutual synchronization of spin torque nano-oscillators through a long-range and tunable electrical coupling scheme, Nat. Commun. **8**, 15825 (2017).

[14] A. Awad, P. Dürrenfeld, A. Houshang, M. Dvornik, E. Iacocca, R. Dumas, and J. Åkerman, Long-range mutual synchronization of spin Hall nano-oscillators, Nat. Phys. **13**, 292 (2017).

[15] A. Kumar, H. Fulara, R. Khymyn, A. Litvinenko, M. Zahedinejad, M. Rajabali, X. Zhao, N. Behera, A. Houshang, A. A. Awad *et al.*, Robust mutual synchronization in long spin Hall nano-oscillator chains, Nano Lett. **23**, 6720 (2023).

[16] S. Bonetti, P. Muduli, F. Mancoff, and J. Åkerman, Spin torque oscillator frequency versus magnetic field angle: The prospect of operation beyond 65 GHz, Appl. Phys. Lett. **94**, 102507 (2009).

[17] R. Cheng, D. Xiao, and A. Brataas, Terahertz antiferromagnetic spin Hall nano-oscillator, Phys. Rev. Lett. **116**, 207603 (2016).

[18] R. Khymyn, I. Lisenkov, V. Tiberkevich, B. A. Ivanov, and A. Slavin, Antiferromagnetic THz-frequency Josephson-like oscillator driven by spin current, Sci. Rep. **7**, 43705 (2017).

[19] O. R. Sulymenko, O. V. Prokopenko, V. S. Tiberkevich, A. N. Slavin, B. A. Ivanov, and R. S. Khymyn, Terahertz-frequency spin Hall auto-oscillator based on a canted antiferromagnet, Phys. Rev. Appl. **8**, 064007 (2017).

[20] Ø. Johansen and A. Brataas, Spin pumping and inverse spin Hall voltages from dynamical antiferromagnets, Phys. Rev. B **95**, 220408(R) (2017).

[21] O. Gomonay, V. Baltz, A. Brataas, and Y. Tserkovnyak, Antiferromagnetic spin textures and dynamics, Nat. Phys. **14**, 213 (2018).

[22] V. Puliafito, R. Khymyn, M. Carpentieri, B. Azzerboni, V. Tiberkevich, A. Slavin, and G. Finocchio, Micromagnetic modeling of terahertz oscillations in an antiferromagnetic material driven by the spin Hall effect, Phys. Rev. B **99**, 024405 (2019).

[23] D.-K. Lee, B.-G. Park, and K.-J. Lee, Antiferromagnetic oscillators driven by spin currents with arbitrary spin polarization directions, Phys. Rev. Appl. **11**, 054048 (2019).

[24] R. E. Troncoso, K. Rode, P. Stamenov, J. M. D. Coey, and A. Brataas, Antiferromagnetic single-layer spin-orbit torque oscillators, Phys. Rev. B **99**, 054433 (2019).

[25] A. Parthasarathy, E. Cogulu, A. D. Kent, and S. Rakheja, Precessional spin-torque dynamics in biaxial antiferromagnets, Phys. Rev. B **103**, 024450 (2021).

[26] E. Gomonay and V. Loktev, Spintronics of antiferromagnetic systems, Low Temp. Phys. **40**, 17 (2014).

[27] V. Baltz, A. Manchon, M. Tsoi, T. Moriyama, T. Ono, and Y. Tserkovnyak, Antiferromagnetic spintronics, Rev. Mod. Phys. **90**, 015005 (2018).

[28] E. G. Galkina and B. A. Ivanov, Dynamic solitons in antiferromagnets, Low Temp. Phys. **44**, 618 (2018).

[29] J. R. Hortensius, D. Afanasiev, M. Matthiesen, R. Leenders, R. Citro, A. V. Kimel, R. V. Mikhaylovskiy, B. A. Ivanov, and A. D. Caviglia, Coherent spin-wave transport in an antiferromagnet, Nat. Phys. **17**, 1001 (2021).

[30] E. A. Turov, A. V. Kolchanov, V. V. Men'shenin, I. F. Mirsaev, and V. V. Nikolaev, *Symmetry and Physical Properties of Antiferromagnets* (Fizmatlit, Moscow, 2001) (CISP - Cambridge International Science Publishing, Cambridge, UK, 2010).

[31] M. Hamdi and D. Grundler, Terahertz slonczewski propagating spin waves and large output voltage in antiferromagnetic spin-Hall nano-oscillators, arXiv:2206.07844.

[32] R. V. Ovcharov, E. G. Galkina, B. A. Ivanov, and R. S. Khymyn, Spin Hall nano-oscillator based on an antiferromagnetic domain wall, Phys. Rev. Appl. **18**, 024047 (2022).

[33] R. V. Ovcharov, B. A. Ivanov, J. Åkerman, and R. S. Khymyn, Antiferromagnetic Bloch line driven by spin current as room-temperature analogue of a fluxon in a long Josephson junction, Phys. Rev. Appl. **20**, 034060 (2023).

[34] I. V. Bar'yakhtar and B. A. Ivanov, Dynamic solitons in a uniaxial antiferromagnet, Zh. Eksp. Teor. Fiz. **85**, 328 (1983) [Sov. Phys. - JETP **39**, 190 (1983)].

[35] E. G. Galkina, R. V. Ovcharov, and B. A. Ivanov, Precessional one-dimensional solitons in antiferromagnets with low dynamic symmetry, Low Temp. Phys. **43**, 1283 (2017).

[36] See Supplemental Material at http://link.aps.org/supplemental/10.1103/PhysRevB.109.L140406 for the detailed AFM model, collective coordinate approach for an AFM DW and the perturbation theory of propagating SWs.

[37] N. J. Whitehead, S. A. R. Horsley, T. G. Philbin, A. N. Kuchko, and V. V. Kruglyak, Theory of linear spin wave emission from a Bloch domain wall, Phys. Rev. B **96**, 064415 (2017).

[38] S. K. Kim, Y. Tserkovnyak, and O. Tchernyshyov, Propulsion of a domain wall in an antiferromagnet by magnons, Phys. Rev. B **90**, 104406 (2014).

[39] A. Vansteenkiste, J. Leliaert, M. Dvornik, M. Helsen, F. Garcia-Sanchez, and B. Van Waeyenberge, The design and verification of MUMAX3, AIP Adv. **4**, 107133 (2014).

[40] N. Koshizuka and K. Hayashi, Raman scattering from magnon excitations in $RFeO_3$, J. Phys. Soc. Jpn. **57**, 4418 (1988).

[41] H. Wijn, 5.5.8.9 DyFeO{3} compounds, in *Perovskites II, Oxides with Corundum, Ilmenite and Amorphous Structures*, edited by H. Wijn, Landolt-Börnstein, Group III Condensed Matter Vol. 27F3 (Springer, Berlin, 1994), pp. 125–134.

[42] X. Fu, X. Liu, and J. Zhou, Terahertz spectroscopic observation of spin reorientation induced antiferromagnetic mode softening in $DyFeO_3$ ceramics, Mater. Lett. **132**, 190 (2014).

[43] E. V. Gomonai, B. A. Ivanov, V. A. L'vov, and G. K. Oksyuk, Symmetry and dynamics of domain walls in weak ferromagnets, Zh. Eksp. Teor. Fiz. **97**, 307 (1990) [Sov. Phys. JETP **70**, 174 (1990)].